Ge Crystals on Si Show Their Light

F. Pezzoli,[1,*] F. Isa,[2] G. Isella,[2] C. V. Falub,[3] T. Kreiliger,[3] M. Salvalaglio,[1] R. Bergamaschini,[1] E. Grilli,[1] M. Guzzi,[1] H. von Känel,[3] and L. Miglio[1]

[1]*LNESS and Dipartimento di Scienza dei Materiali, Università degli Studi di Milano-Bicocca, via Roberto Cozzi 55, I-20125 Milano, Italy*

[2]*LNESS and Dipartimento di Fisica, Politecnico di Milano, Piazza Leonardo da Vinci 32, I-20133 Milano, Italy*

[3]*Laboratory for Solid State Physics, ETH Zürich, Schafmattstrasse 16, CH-8093 Zürich, Switzerland*

(Received 17 March 2014; revised manuscript received 28 April 2014; published 28 May 2014)

We report micron-sized Ge crystal arrays grown on deeply patterned Si substrates that yield a surge of the interband photoluminescence intensity by more than 2 orders of magnitude with respect to that typical for epitaxial layers directly grown on planar substrates. This finding is ascribed to the strongly modified internal quantum efficiency induced by controlling the nonradiative recombination at dislocations and to the improved light extraction offered by the array architecture. By spectrally resolving the interband and the dislocation-related luminescence, we address the parasitic activity of extended defects and its impact on the optical properties of the heterosystem. Such results are then exploited along with band gap engineering to design SiGe reflectors and Ge quantum wells that are effective in further amplifying the emission yield.

DOI: 10.1103/PhysRevApplied.1.044005

I. INTRODUCTION

In recent years, intensive investigations have been pursued to promote more efficient radiative recombination in Ge [1–10]. Most of them rely on early proposals of inducing an indirect-to-direct gap transition by tensile strain [11] or Sn alloying [12]. Less attention, however, has been paid to the control over the spontaneous emission properties of this semiconductor. As soon recognized [13], the quantum efficiency of the radiative emission is very poor, and the lifetime of photoexcited carriers is easily affected by structural imperfections: a remarkably severe bottleneck in heterostructures. The Ge/Si heterosystem is, indeed, prone to the injection of misfit dislocations [14]. Such defects extend to the free surface via threading arms reducing the internal quantum efficiency (IQE) of the photon-emitting medium [15–17].

Here we address this issue by taking advantage of high aspect-ratio Ge crystals termed here as towers, epitaxially grown on top of micron-sized Si pillars in a maskless process [18–20]. Photoluminescence (PL) experiments and modeling of carrier diffusion and recombination demonstrate a strong enhancement of the interband (IB) emission in these heteroepitaxial architectures. We explain such finding as due to the complete removal of threading dislocations (TDs) and the reduced loss of light offered by the tower configuration. A result that can be extended to other heterosystems.

[*]Corresponding author.
fabio.pezzoli@unimib.it

II. Ge ON Si(001) HETEROEPITAXY

We first discuss how to control dislocations in the Ge/Si system. Figures 1(a)–1(c) show the morphology of 8-μm-tall Ge towers grown at a rate of 4.2 nm/s and a temperature of 550 °C by low-energy plasma enhanced chemical vapor deposition [21]. The growth is performed onto 2×2 μm^2, 5×5 μm^2, and 9×9 μm^2 pillars prepared by optical lithography and deep reactive ion etching in Si(001) substrates yielding tower arrays with surface filling factor of 77%, 89%, and 90%, respectively [18,20]. The deposited material is intentionally undoped, and the residual background doping of the samples is determined by room temperature Hall measurements to be p type and equal to $(4.2 \pm 0.8) \times 10^{15}$ cm^3. All the samples are grown one after the other to ensure the same residual doping level.

The selective deposition on Si pillars results in Ge towers with a top surface bounded by {113} and (001) facets. The latter is at the center of the tower, and it shrinks by decreasing the width of the pillar base, as shown in Fig. 1(d). Since vertical and slanted dislocations are pinned by the growth front [18,22], the TDs are deflected towards the lateral sidewalls by the inclined {113} facets and eventually expelled [23]. Etch-pit counting measurements summarized in the insets of Fig. 1 confirm that the portion of the overall volume of a Ge tower containing TDs is determined by the (001) top facet [18,23]. Noticeably, for Ge towers with a pyramidal top surface bounded by {113} facets, the TDs are fully expelled within the first microns from the buried Ge/Si interface so that the upper part of the tower remains free from defects [18,23]. In the patterned region, the density of TDs can, thus, be tuned from zero up to the values of the continuous Ge film deposited during the same growth run on

 © 2014 American Physical Society

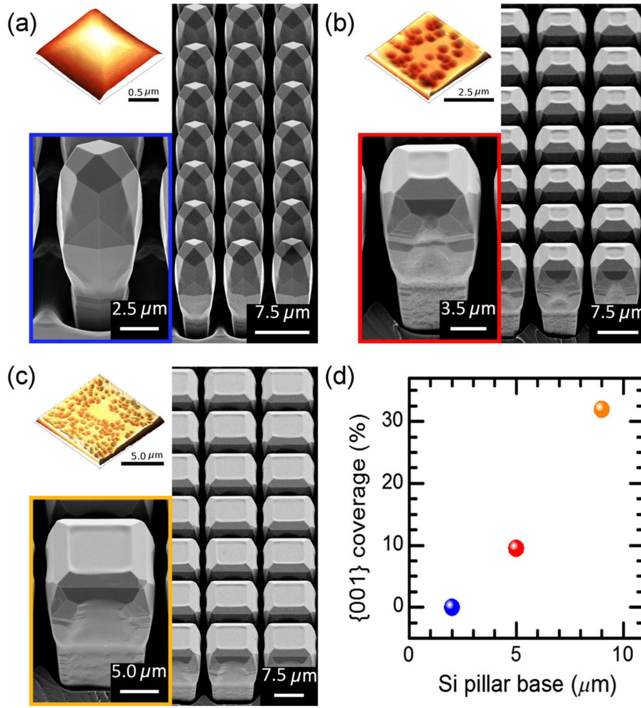

FIG. 1. Perspective-view scanning electron microscope (SEM) micrographs of the 8-μm Ge towers grown on (a) 2×2 μm^2, (b) 5×5 μm^2, and (c) 9×9 μm^2 Si(001) pillars. The insets show atomic force microscopy images of the top surface of the Ge towers after selective defect etching. Threading dislocations are visible as conical valleys. (d) Top surface coverage of the (001) facet as a function of the base size of the pristine Si pillars.

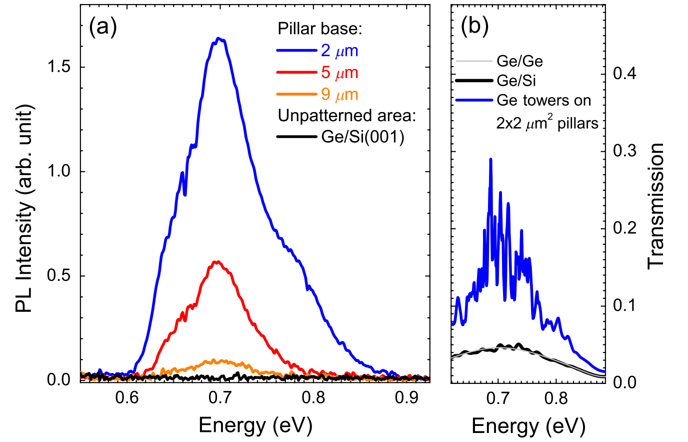

FIG. 2. (a) Room temperature PL spectra of Ge towers grown on Si pillars having a square base of 2×2 μm^2 (blue line), 5×5 μm^2 (red line), 9×9 μm^2 (orange line), and Ge grown on flat Si(001) surface (black line). (b) The 2D finite-difference time-domain results for the power transmitted through the Ge/air interface for Ge towers on 2×2 μm^2 Si pillars (blue line), an 8-μm-thick continuous Ge/Si heterostructure (black line), and a Ge/Ge homostructure (gray line).

the flat Si substrate by simply changing the size of the Si pillar base while keeping the growth parameters fixed.

III. ROOM TEMPERATURE PL EXPERIMENTS ON Ge TOWERS

PL measurements are carried out in the 6–300 K temperature range using a closed-cycle cryostat and a Fourier transform spectrometer equipped with a PbS detector. A continuous wave Nd-YVO_4 laser operated at 1.165 eV is used as the excitation source. The laser spot size on the sample surface has a diameter of approximately 100 μm, and the corresponding power density is between 1 and 3 kW/cm^2.

Figure 2(a) shows the room temperature (RT) PL spectra of Ge-tower arrays. The corresponding spectrum recorded in the unpatterned area of the same sample is shown for comparison as a black line. Continuous Ge films directly deposited on Si have a very poor external quantum efficiency (EQE) for the following two reasons. First, a large fraction of the light generated inside the Ge epilayer is guided in the Ge slab and remains trapped by total internal reflection, thus, limiting the light extraction efficiency (LEE). Second, the large number of defects in the continuous Ge film above the unpatterned substrate areas has a severe impact on the IQE, since the carrier dynamics is dictated by parasitic nonradiative channels. The time scale for these processes is much shorter than that of the radiative IB transitions. As a result, the luminescence intensity falls well below the measurement noise, as shown by the black line in Fig. 2(a). This is in agreement with reports on typical undoped Ge/Si heteroepitaxial layers, where no PL signal can be detected in as-grown samples [17]. By contrast, Fig. 2(a) reveals a rapid increase of the PL intensity for as-grown Ge towers with decreasing size.

Fully faceted Ge towers on 2×2 μm^2 Si pillars yield a massive increase in the EQE, since the emission intensity is more than 2 orders of magnitude larger than the noise level of the corresponding continuous film [24]. We also note that the interband emission intensity in Ge towers grown on 2×2 μm^2 Si pillars turns out to be comparable to the PL intensity of dislocation-free Ge wafers [25,26]. This unexpected emission enhancement is achieved without the need of postgrowth annealing and without any surface treatment ensuring a low surface recombination velocity, despite the large surface-to-volume ratio and small surface coverage of the arrays.

IV. LIGHT EMISSION ENHANCEMENT IN Ge TOWERS

In Ge towers, the sidewalls will bounce off most of the light emitted outside the critical angle for total internal reflection. This emission being guided to the top surface can possibly be outcoupled to the air with a high directionality. The selective growth on deeply patterned substrates offers a greatly simplified solution for light

extraction over approaches relying on more complex photonic crystal designs [27,28].

In order to fully quantify the effect of surface texture in determining both the effective light path in the towers and the extraction efficiency of the emitted light, we employ a 2D finite-difference time-domain (FDTD) method [29]. By following the correspondence principle, we model the spontaneous radiative recombination from electrons and holes in Ge by classic electric dipole moments oriented parallel to the direction of the valence band p orbitals. The optical response of the Ge-based heterostructures to photons emitted at the energy of the direct and indirect gaps is investigated by using a broadband source covering the range from 1.4 μm (0.885 eV) to 2 μm (0.620 eV) and calculating the transmission towards the exterior of the heterostructure. To better capture the incoherent nature of the radiative emission, we average over separate simulation runs of the same dipole oriented along the x, y, and z axes and in different positions along the height of the Ge layer, i.e., 1, 4, and 7 μm from the Ge/Si interface. In the FDTD simulations, perfectly matched layer boundary conditions are used. The structure is designed to consist of Ge towers on 2-μm-wide Si pillars. The Ge towers have a triangular $\{113\}$ apex, a width of 4 μm, and a height of 8 μm. The simulated region contains at least three periods (pitch of 5 μm), and the dipoles are located in the central tower to avoid coherence effects. In addition, we keep the dimensions of the simulation cell fixed and model as benchmarks also an 8-μm-thick homogeneous Ge/Si heterostructure and an 8-μm-thick Ge/Ge homostructure.

As shown by the thin solid gray line in Fig. 2(b), the outcoupled light emitted from dipoles buried below the surface of the Ge/Ge reference sharply decreases in the high-energy range due to the onset of direct gap absorption. In addition, FDTD shows that, for the dipole distribution considered here, the light emitted from an 8-μm Ge/Si epilayer is the same as in the Ge/Ge reference, although it is modulated in the transparency range of the indirect gap [see black line in Fig. 2(b)]. This is due to multiple reflections induced by the change in the refractive index at the buried Ge/Si interface, which, on the contrary, is not present in the Ge/Ge homostructure.

Noticeably, the solid blue line of Fig. 2(b) demonstrates that the fraction of emitted power that escapes into the detection solid angle is larger in the Ge towers than in continuous Ge/Si films, provided that the layer thickness is the same. In particular, in the considered wavelength range, a LEE enhancement of 2.9 ± 0.9 is obtained by the ratio between the transmitted power for Ge towers grown on 2×2 μm^2 Si pillars and that of the unpatterned Ge/Si layer. The almost constant LEE in the interband emission range [30] suggests, in addition, that self-absorption of direct gap emission in the Ge towers is comparable with the self-absorption taking place in a continuous Ge on Si layer having the same thickness. It is worth noting that the removal of the triangular apex, so as to mimic the optical response of flat-topped towers, does not appreciably change the results discussed above.

For Ge towers grown on 2×2 μm^2 Si pillars, the LEE is about 3 times as large as that of an unpatterned Ge/Si layer. This value cannot, thus, explain the EQE experimentally observed in the Ge towers. The largest fraction of the aforementioned EQE enhancement must be, therefore, attributed to an increase of the IQE, as a result of the suppression of the parasitic nonradiative recombination channels related to the dislocations.

V. TEMPERATURE DEPENDENCE OF INTERBAND AND DISLOCATION RELATED LUMINESCENCE

Although the spontaneous emission of epitaxial Ge towers carries the fingerprints of defect-free material, the dislocations present in the first few microns close to the interface can still play a non-negligible role. In order to shed light on the influence of dislocations on the carrier population in the bands, we perform temperature-dependent PL measurements on Ge towers bounded by $\{113\}$ facets summarized in Fig. 3(a). The wide spectral range covered by the measurements allows us to extend the optical investigations well below the low-energy edge of the Ge emission and to study the interplay between IB recombination and dislocation-related PL (DPL). At 6 K, it can be clearly seen that the PL spectrum is characterized by direct gap recombination at 0.882 eV [31], indirect gap recombination assisted by longitudinal acoustic phonon emission at 0.712 eV, and the no-phonon line at 0.736 eV [32]. The additional band extending from 0.45 eV to about 0.67 eV is attributed to recombination taking place at dislocations [33–36].

Figure 3(b) shows the integrated PL intensity of dislocation and IB emission (direct plus indirect gap transitions) versus temperature T. Interestingly, the IB luminescence exhibits two temperature regimes. By increasing the temperature, the PL decreases gradually, but above a critical temperature, $T_C \approx 125$ K, it rises sharply. For $T > T_C$, the abrupt DPL quenching occurs in phase with the steep increase of the IB emission. In order to obtain a more detailed understanding of the observed trends, we employ the following charge-dependent potential barrier model. See Refs. [26,37,38] for a full discussion. Under steady state conditions, expressions for the net concentrations δm of holes trapped at dislocations, for the excess concentration δn of electrons in the conduction band, and for the excess hole concentration δp in the valence band can be derived from rate equations involving a potential barrier between charged line defects and the semiconductor [26,38,39]. At a finite temperature, trapped carriers can either be released and contribute to the radiative IB recombination, or contribute to the DPL emission, or recombine nonradiatively at the dislocation site. The inset of Fig. 3(b) illustrates the physical processes involved.

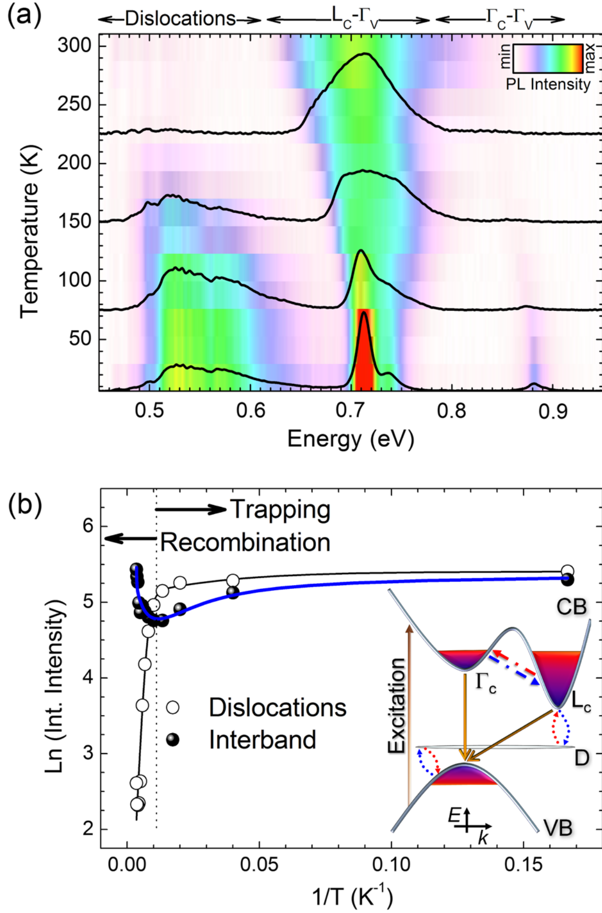

FIG. 3. (a) Contour plot of the temperature-dependent PL for Ge towers grown on 2×2 μm^2 Si pillars. Spectra at 6, 75, 150, and 225 K are superimposed as references. (b) Integrated intensity of the interband emission (direct plus indirect) and dislocation band as a function of temperature. The blue solid line is the result of charge-dependent barrier modeling. The black solid line is the fitting curve based on an Arrhenius function with two activation energies [26]. The recombination and trapping regimes are separated by a black dotted vertical line. The inset is a sketch of the luminescence processes taking place in the Ge samples.

As shown in Fig. 3 by the solid blue line obtained by the model, the IB transition is well described by applying the constraint of crystal neutrality [38], $\delta n = \delta p + \delta m$. According to the model, at low temperatures $\delta p \ll \delta m$, since carriers leak out from the band into the trapping defect levels, thereby enhancing the defect emission. When the temperature is increased, the traps are emptied by thermal activation, such that $\delta p \gg \delta m$. In other words, the IB recombination regime takes over, and the IB luminescence becomes dominant. The temperature T_c at which the crossing between the recombination and trapping regimes takes place coincides with the temperature at which $\delta p = \delta m$, and the IB integrated intensity has a minimum [38], as observed in the experimental data of Fig. 3(b).

VI. ENHANCEMENT OF INTERBAND EMISSION VIA BAND GAP ENGINEERING

Having unraveled the optical activity of dislocations present in the region closest to the buried interface of epitaxial Ge towers, we use band gap engineering to minimize their role. Based on the band alignments, effective masses, and deformation potentials from Refs. [40,41], we take as an ansatz a sample at room temperature and calculate the transmission coefficients for electrons and holes through a $Si_{1-x}Ge_x$ barrier within the transfer matrix formalism [42,43].

Figure 4(a) shows the transmitted fraction of carriers versus Ge content x of a $Si_{1-x}Ge_x$ reflector. The fraction of transmitted holes increases monotonically with x as a result of the decreasing valence band edge offset [26]. Surprisingly, the transmitted fraction of electrons first decreases with increasing x and then slowly increases again. This counterintuitive prediction can be rationalized as a result of the crossover between the Δ and L valleys of the SiGe band structure under tensile strain [26].

Since, as summarized in Fig. 4(a), the alloy concentration required for optimum performance of these reflectors is around the minimum of the transmission probability for electrons, we grow three samples with Ge towers on 2-μm-wide Si pillars with 10-nm-thick $Si_{0.25}Ge_{0.75}$ barriers introduced at a distance of 6 μm (A), 4 μm (B), and 2 μm

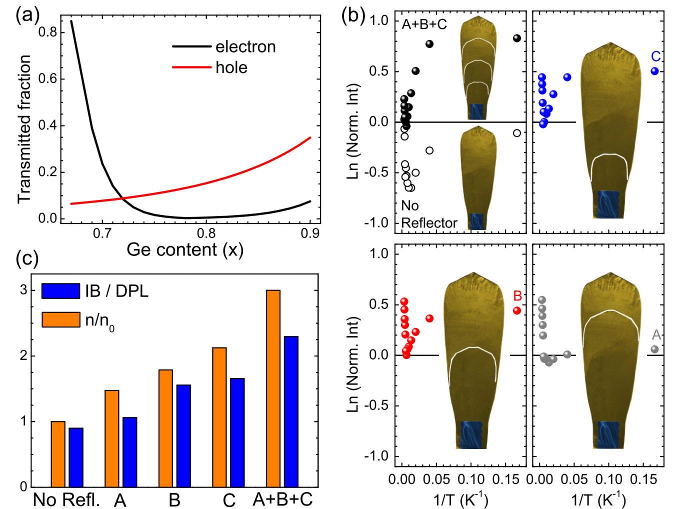

FIG. 4. (a) Transmission current for electrons (black) and holes (red) through a 10-nm-thick $Si_{1-x}Ge_x$ reflector as a function of the Ge content of the alloy layer. (b) Integrated intensity of the IB emission of Ge towers as a function of the temperature for towers without (no reflector) and with $Si_{0.25}Ge_{0.75}$ reflectors at 2 (A), 4 (B), and 6 (C) μm from the top surface according to the schemes in the insets. IB data are normalized for each sample to the corresponding DPL integrated intensity at 6 K. (c) Calculated number of carriers n (orange bars) in Ge towers normalized to the value n_0 of the tower with no reflectors. Blue bars are the IB-to-DPL ratio measured at 6 K. Data are reported for the different $Si_{0.25}Ge_{0.75}$ reflectors.

(C) from the dislocated Si/Ge interface. Finally, a fourth sample contains all three barriers. The thickness of the $Si_{0.25}Ge_{0.75}$ reflectors is optimized so that plastic strain relaxation is avoided. Figure 4(b) shows the IB integrated intensity of the Ge towers. At low temperature and in the trapping regime, the spectral weight of the PL bands is modulated by optical recombination centers and traps competing for the capture of carriers. Figure 4(b) clearly demonstrates that the SiGe reflectors improve the radiative transitions across the Ge gaps, confirming that the dislocations in the interfacial region are responsible for the PL quenching of the IB emission. The role of SiGe reflectors as blocking layers is further clarified by the calculations of carrier diffusion summarized in Fig. 4(c).

We model the distribution of minority excess carriers in Ge towers by including the dislocation recombination at the bottom of the towers, as follows. Under light excitation, the carriers are generated at the top surface of each illuminated Ge tower within a volume defined by the width of the tower and the laser penetration depth in Ge. During the thermalization process and before radiative recombination, the photoinjected carriers diffuse inside the material. Ge towers, at a first approximation, have cylindrical symmetry so that the excess carrier dynamics can be treated as a one-dimensional diffusion problem along the tower axis z. For the sake of simplicity, unipolar diffusion is assumed and exciton formation is neglected. The illuminated surface is defined at $z = 0$.

The final sample volume probed by PL experiments depends on the diffusion length defined as $L = \sqrt{D\tau}$. In Ge, typical values of radiative lifetime $\tau_r \approx 30$ μs, and diffusion constant $D \approx 65$ cm^2/s (see Ref. [17] and references therein) yield L, which is about 50 times larger than the tower height. As a consequence, under continuous wave illumination and in the absence of nonradiative recombination centers, the carriers will be homogeneously distributed within the whole volume of the Ge tower. On the other hand, once the dislocation activity is turned on, the carriers generated at the illuminated top surface of the tower quickly diffuse to its bottom where they can recombine at the buried dislocations [44]. The calculation results summarized by the dashed gray line in Fig. 5 show an almost uniform excess carrier density through the whole tower with a shallow decrease of carrier density along the tower height. It should be noted that the latter is below 0.1% and, thus, not appreciable in the graph [26].

The role of a SiGe reflector embedded into the Ge tower can finally be modeled by assuming, according to the calculations reported in Fig. 4(a), $P \sim 7\%$ as an average value of electron and hole transmission probabilities evaluated at the actual Ge content of the barrier. The carrier distribution we obtain when a single barrier is at $z = 2$ and 6 μm from the top surface of the tower is shown by the solid lines in Figs. 5(a) and 5(b), respectively. Since the barrier has low transmittance, a higher injection level of

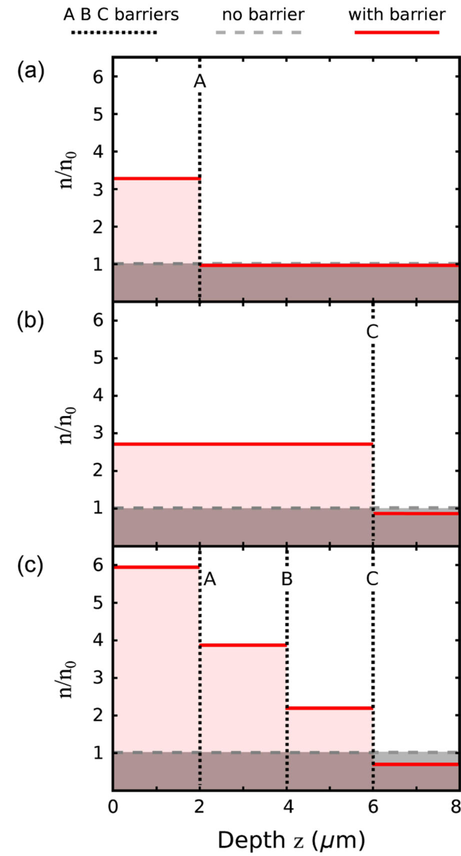

FIG. 5. Calculated carrier distribution at steady state in Ge towers embedding (a) a single SiGe barrier at 2 μm, (b) a single SiGe barrier at 6 μm, and (c) three SiGe barriers at 2, 4, and 6 μm from the Ge-tower top surface at $z = 0$. The carrier profile with no barrier (dashed line) is shown for comparison. All density values are normalized with respect to the constant carrier density value n_0 obtained for the tower without barriers.

carriers can be obtained in the upper part of the Ge tower, while on the lower part of the tower, the carrier density is limited to low values because of the dislocation sink. Remarkably, by comparing Figs. 5(a) and 5(b), it turns out that the integral of the carrier density is higher when the barrier is closer to the bottom of the Ge tower. Moreover, when more than one reflector is introduced, the number of carriers is further enhanced due to the superposition of single barrier effects: a higher density of carriers is reached, and the dislocation sink effect is weakened being active only on the small portion of carriers reaching the bottom Ge/Si interface. This is evident in Fig. 5(c), where the carrier distribution for a tower with three barriers at $z = 2$, 4, and 6 μm is shown.

The model outlined here, although simple, captures completely the qualitative impact of SiGe barriers on carrier population and provides a theoretical framework for the experimental findings summarized in Fig. 4(b). The calculations demonstrate that as the SiGe layer is pushed towards the dislocated interface, the number of carriers

within the overall volume of the Ge tower increases, thus, incrementing the IB recombination. Noteworthy, the largest improvement of the IB-to-DPL ratio is achieved for the sample with three embedded SiGe reflectors since this configuration is most efficient in suppressing the carrier depletion by the buried defects.

VII. OPTICAL PROPERTIES OF QUANTUM WELL TOWERS

In a final attempt to confine carriers away from the dislocated buried interface, we employ a larger number of SiGe reflectors acting as Ge-rich barriers for pure Ge quantum wells (QWs). The sample investigated here is a strain-symmetrized structure with a type I band alignment [1,45–48]. It consists of 50 Ge QWs embedded in $Si_{0.15}Ge_{0.85}$ barriers deposited on top of an 8-μm-thick $Si_{0.1}Ge_{0.9}$ buffer on a $2 \times 2\ \mu m^2$ Si array.

The SEM micrographs reported in Figs. 6(a) and 6(b) show that the QW crystals are bounded by $\{113\}$ facets and that the typical morphology of fully faceted towers is not affected by the presence of the heterostructures. The high-resolution x-ray diffraction measurements shown in Fig. 6(c) confirm that the SiGe buffer is fully relaxed and that the QW structure is lattice matched to the top of the buffer, which contains $(91 \pm 1)\%$ of Ge. In the (004) reciprocal space map of Fig. 6(c), the coherent Ge QWs grown on high-index $\{113\}$ facets give rise to diffraction maxima (red arrows) along the dashed [001] and [113] lines. The structural parameters of the QW stack in the towers are deduced from the spacing of these diffraction peaks. The Ge content of the barrier is $(86 \pm 1)\%$, while the thickness of the QW and barrier is about 15 and 23 nm, respectively. A second kind of satellite depicted by green arrows along the [001] line in Fig. 6(c) arises from the thermally strained QW present in the trenches between neighboring pillars. On the contrary, the QW towers are free from thermal strain, as expected from aspect-ratio reasons [18,20].

In Fig. 6(d), the low-temperature PL of QW towers is compared with the negligible PL of the reference structure deposited outside the pattern during the same growth. Remarkably, DPL dominates the spectrum measured on the unpatterned areas but is strongly suppressed in the QW towers. Here, quantum-confined transitions related to the direct gap at the Γ point and the indirect gap at the L point of the Ge QWs are clearly visible. We attribute the PL peak at 0.959 eV to the fundamental transition between the confined state at the Γ point in the conduction band and the heavy hole subband, namely, $c\Gamma 1$-HH1. The low-energy PL doublet is ascribed to dipole-allowed transitions across the indirect gap. The high-energy part of the doublet at 0.745 eV is possibly due to the $cL1$-HH1 recombination of confined carriers, while the line at 0.722 eV is the phonon-assisted optical transition. Such values are in agreement with transition energies reported in the literature

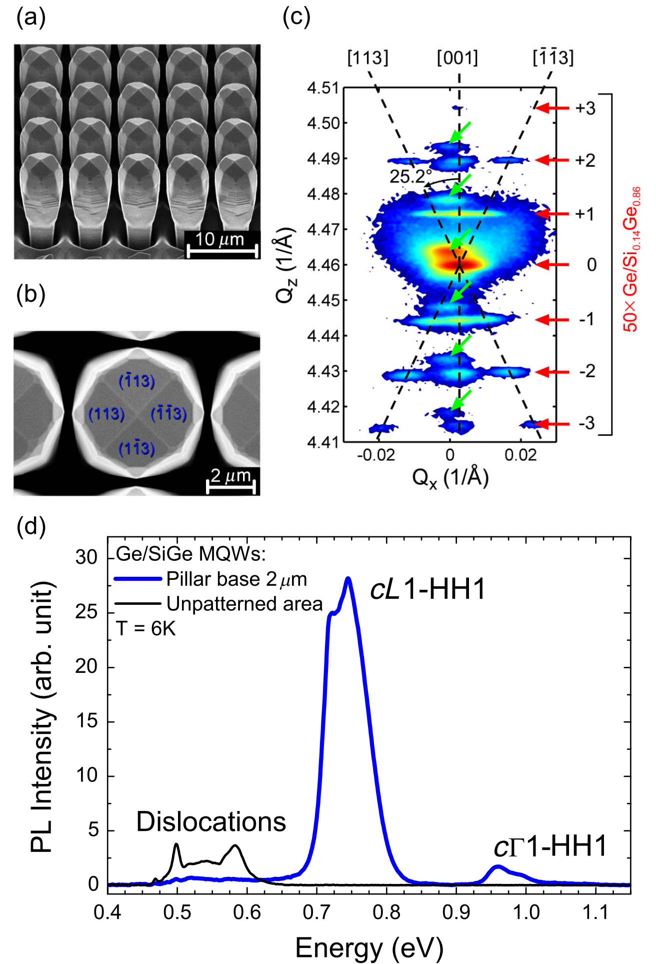

FIG. 6. (a) Perspective SEM image of Ge/SiGe multiple QW towers grown on 2-μm-wide Si pillars. (b) Top-view SEM micrograph of the QW towers. (c) Reciprocal space map of the QW towers measured around (004) reflection. The superlattice satellite peaks are numbered and indicated by red and green lines. (d) Low-temperature PL for QW towers grown on $2 \times 2\ \mu m^2$ Si pillars (blue curve) and on the unpatterned flat (001)Si region of the same wafer (black curve). Quantum-confined transitions related to the direct gap at the Γ point and the indirect gap at the L point of Ge are shown along with the dislocation-related emission.

for (001)Ge/SiGe QWs grown with the same method and similar deposition parameters [45].

The lack of DPL due to the effective localization of carriers in the defect-free part of the tower suggests a strong emission efficiency for the QW towers. To address this further, we benchmark the optical properties of QW towers against state-of-the-art QWs, namely, 50 strain-symmetrized $Ge/Si_{0.15}Ge_{0.85}$ QWs grown on a graded buffer ending with a $Si_{0.1}Ge_{0.9}$ constant composition layer on an unpatterned Si(001) substrate. We note that for the two QW samples under comparison, the QWs have the same nominal parameters. Details about the growth and the structural data of the benchmark sample of QWs deposited on the graded buffer are reported in Refs. [49,50].

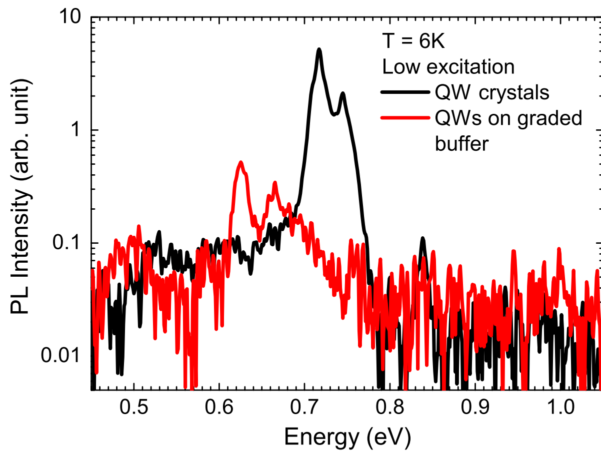

FIG. 7. Low-temperature and low excitation power density PL for QW towers grown on $2 \times 2\ \mu m^2$ Si pillars (black curve) and on a graded virtual substrate (red curve).

The PL experiments are performed under the same experimental conditions and under a low excitation power density, about 4×10^{-2} kW/cm^2, in order to better highlight the differences among the two samples. As it turns out from Fig. 7, in the QW sample grown on a graded buffer, the QW luminescence is quenched, whereas the defect emission below 0.7 eV is still visible. On the contrary, in the QW tower, the PL is dominated above 0.7 eV by the interband emission across the indirect gap. This clearly demonstrates that QW towers, by far, outperform high-quality (001)Ge QWs grown on graded SiGe buffers

VIII. SUMMARY

In conclusion, we show that the Ge/Si tower system is an excellent playground to unfold the physics underlying the various recombination mechanisms effective in heteroepitaxial architectures. The dislocation-related emission, noticeably present in Ge/Si, allows us to underpin the role played by defects in limiting the radiative emission and to identify viable approaches based upon band gap engineering to enhance the optical response. The large improvement in the internal quantum efficiency of the towers, along with the improved light extraction efficiency induced by substrate patterning, is not restricted to Ge and can pave the way to epitaxial, high-brightness, and high-directional light sources on Si.

ACKNOWLEDGMENTS

We thank E. Gatti, E. Bonera, A. Marzegalli, and F. Montalenti for fruitful discussions. This work is supported by Pilegrowth Tech, Regione Lombardia through Dote ricercatori, the Swiss Federal program Nano-Tera through Project NEXRAY, and the EC through the GREEN Silicon Project No. 257750.

[1] M. Virgilio and G. Grosso, Type-I alignment and direct fundamental gap in SiGe based heterostructures, J. Phys. Condens. Matter **18**, 1021 (2006).

[2] V. R. D'Costa, Y. Y. Fang, J. Tolle, J. Kouvetakis, and J. Menéndez, Tunable optical gap at a fixed lattice constant in group-IV semiconductor alloys, Phys. Rev. Lett. **102**, 107403 (2009).

[3] R. Ragan and H. A. Atwater, Measurement of the direct energy gap of coherently strained SnGe/Ge(001) heterostructures, Appl. Phys. Lett. **77**, 3418 (2000).

[4] M. El Kurdi, H. Bertin, E. Martincic, M. de Kersauson, G. Fishman, S. Sauvage, A. Bosseboeuf, and P. Boucaud, Control of direct band gap emission of bulk germanium by mechanical tensile strain, Appl. Phys. Lett. **96**, 041909 (2010).

[5] J. Liu, X. Sun, R. Camacho-Aguilera, L. C. Kimerling, and J. Michel, Ge-on-Si laser operating at room temperature, Opt. Lett. **35**, 679 (2010).

[6] M. d'Avezac, J.-W. Luo, T. Chanier, and A. Zunger, Genetic-algorithm discovery of a direct-gap and optically allowed superstructure from indirect-gap Si and Ge semiconductors, Phys. Rev. Lett. **108**, 027401 (2012).

[7] J. R. Sánchez-Pérez, C. Boztug, F. Chen, F. F. Sudradjat, D. M. Paskiewicz, R. B. Jacobson, M. G. Lagally, and R. Paiella, Direct-bandgap light-emitting germanium in tensilely strained nanomembranes, Proc. Natl. Acad. Sci. U.S.A. **108**, 18893 (2011).

[8] J. R. Jain, A. Hryciw, T. M. Baer, D. A. B. Miller, M. L. Brongersma, and R. T. Howe, A micromachining-based technology for enhancing germanium light emission via tensile strain, Nat. Photonics **6**, 398 (2012).

[9] M. J. Suess, R. Geiger, R. A. Minamisawa, G. Schiefler, J. Frigerio, D. Chrastina, G. Isella, R. Spolenak, J. Faist, and H. Sigg, Analysis of enhanced light emission from highly strained germanium microbridges, Nat. Photonics **7**, 466 (2013).

[10] E. Bonera, M. Bollani, D. Chrastina, F. Pezzoli, A. Picco, O. G. Schmidt, and D. Terziotti, Substrate strain manipulation by nanostructure perimeter forces, J. Appl. Phys. **113**, 164308 (2013).

[11] R. A. Soref and L. Friedman, Direct-gap Ge/GeSn/Si and GeSn/Ge/Si heterostructures, Superlattices Microstruct. **14**, 189 (1993).

[12] E. A. Fitzgerald, P. E. Freeland, M. T. Asom, W. P. Lowe, R. A. Macharrie, B. E. Weir, A. R. Kortan, F. A. Thiel, Y. H. Xie, A. M. Sergent, S. L. Cooper, G. A. Thomas, and L. C. Kimerling, Epitaxially stabilized GeSn diamond cubic alloys, J. Electron. Mater. **20**, 489 (1991).

[13] W. van Roosbroeck and W. Shockley, Photon-radiative recombination of electrons and holes in germanium, Phys. Rev. **94**, 1558 (1954).

[14] C. Claeys and E. Simoen, *Extended Defects in Germanium* (Springer-Verlag, Berlin, 2009).

[15] D. Liang and J. E. Bowers, Recent progress in lasers on silicon, Nat. Photonics **4**, 511 (2010).

[16] S. R. Jan, C.-Y. Chen, C.-H. Lee, S.-T. Chan, K.-L. Peng, C. W. Liu, Y. Yamamoto, and B. Tillack, Influence of defects and interface on radiative transition of Ge, Appl. Phys. Lett. **98**, 141105 (2011).

[17] G. Grzybowski, R. Roucka, J. Mathews, L. Jiang, R. T. Beeler, J. Kouvetakis, and J. Menéndez, Direct versus

indirect optical recombination in Ge films grown on Si substrates, Phys. Rev. B **84**, 205307 (2011).

[18] C. V. Falub, H. von Känel, F. Isa, R. Bergamaschini, A. Marzegalli, D. Chrastina, G. Isella, E. Müller, P. Niedermann, and Leo Miglio, Scaling hetero-epitaxy from layers to three-dimensional crystals, Science **335**, 1330 (2012).

[19] Ge towers with large aspect ratios (height to width), such as the ones discussed in this work, are fully relaxed and unaffected by thermal strain; see Refs. [18,20] for a discussion.

[20] C. V. Falub, M. Meduňa, D. Chrastina, F. Isa, A. Marzegalli, T. Kreiliger, A. G. Taboada, G. Isella, Leo Miglio, A. Dommann, and H. von Känel, Perfect crystals grown from imperfect interfaces, Sci. Rep. **3**, 2276 (2013).

[21] C. Rosenblad, H. R. Deller, A. Dommann, T. Meyer, P. Schröter, and H. von Känel, Silicon epitaxy by low-energy plasma enhanced chemical vapor deposition, J. Vac. Sci. Technol. A **16**, 2785 (1998).

[22] J. Bai, J. S. Park, Z. Cheng, M. Curtin, B. Adekore, M. Carroll, A. Lochtefeld, and M. Dudley, Study of the defect elimination mechanisms in aspect ratio trapping Ge growth, Appl. Phys. Lett. **90**, 101902 (2007).

[23] A. Marzegalli, F. Isa, H. Groiss, E. Müller, C. V. Falub, A. G. Taboada, P. Niedermann, G. Isella, F. Schäffler, F. Montalenti, H. von Känel, and M. Leo, Unexpected dominance of vertical dislocations in high-misfit Ge/Si(001) films and their elimination by deep substrate patterning, Adv. Mater. **25**, 4408 (2013).

[24] The interband emission intensity is a factor of approximately 300 and 700 times above the noise level of the corresponding continuous film for an excitation power density of about 1 and 3 kW/cm^2, respectively.

[25] A direct comparison is provided by the integrated intensity measured at RT in Ge towers [Fig. 3(b)] and in a Ge wafer [Fig. S1 of the Supplemental Material [26]].

[26] See the Supplemental Material at http://link.aps.org/supplemental/10.1103/PhysRevApplied.1.044005 for technical details of the experiment and the model analysis.

[27] P. Boucaud, M. El Kurdi, S. David, X. Checoury, X. Li, T.-P. Ngo, S. Sauvage, D. Bouchier, G. Fishman, O. Kermarrec, Y. Campidelli, D. Bensahel, T. Akatsu, C. Richtarch, and B. Ghyselen, Germanium-based nanophotonic devices: Two-dimensional photonic crystals and cavities, Thin Solid Films **517**, 121 (2008).

[28] C. Boztug, J. R. Sánchez-Pérez, J. Yin, M. G. Lagally, and R. Paiella, Grating-coupled mid-infrared light emission from tensiley strained germanium nanomembranes, Appl. Phys. Lett. **103**, 201114 (2013).

[29] We perform the numerical calculations by using a commercial program from Lumerical.

[30] The enhancement is 2.6 ± 0.6 and 3 ± 1 in the 1.4–1.7 μm and 1.7–2 μm range, respectively.

[31] F. Pezzoli, L. Qing, A. Giorgioni, G. Isella, E. Grilli, M. Guzzi, and H. Dery, Spin and energy relaxation in germanium studied by spin-polarized direct-gap photoluminescence, Phys. Rev. B **88**, 045204 (2013).

[32] R. R. Lieten, K. Bustillo, T. Smets, E. Simoen, J. W. Ager, E. E. Haller, and J. P. Locquet, Photoluminescence of bulk germanium, Phys. Rev. B **86**, 035204 (2012).

[33] A. I. Kolyubakin, Yu. A. Osip'yan, S. A. Shevchenko, and E. A. Shteinman, Dislocation luminescence in Ge, Fiz. Tverd. Tela (Leningrad) **26**, 677 (1984) [Sov. Phys. Solid State **26**, 407 (1984)].

[34] A. I. Kolyubakin, Y. A. Ossipyan, S. A. Shevchenko, and E. A. Steinman, On the energy-spectrum of dislocations in germanium, Acta Phys. Pol. A **69**, 409 (1986).

[35] Y. S. Lelikov, Y. T. Rebane, and Y. G. Shreter, Optical-properties of dislocations in germanium-crystals, Inst. Phys. Conf. Ser. **104**, 119 (1989).

[36] A. N. Izotov, A. I. Kolyubakin, S. A. Shevchenko, and E. A. Steinman, Photoluminescence and splitting of dislocations in germanium, Phys. Status Solidi (a) **130**, 193 (1992).

[37] S. Roy Morrison, Recombination of electrons and holes at dislocations, Phys. Rev. **104**, 619 (1956).

[38] T. Figielski, Recombination at dislocations, Solid State Electron. **21**, 1403 (1978).

[39] R. Labusch and J. Hess, Photoconductivity at dislocations in germanium, Phys. Status Solidi (a) **146**, 145 (1994).

[40] M. M. Rieger and P. Vogl, Electronic-band parameters in strained $Si_{1-x}Ge_x$ alloys on $Si_{1-y}Ge_y$ substrates, Phys. Rev. B **48**, 14276 (1993).

[41] D. J. Paul, 8-band kp modeling of the quantum confined stark effect in Ge quantum wells on Si substrates, Phys. Rev. B **77**, 155323 (2008).

[42] R. Tsu and L. Esaki, Tunneling in a finite superlattice, Appl. Phys. Lett. **22**, 562 (1973).

[43] J. J. Finley, R. J. Teissier, M. S. Skolnick, J. W. Cockburn, G. A. Roberts, R. Grey, G. Hill, M. A. Pate, and R. Planel, Role of the X minimum in transport through AlAs single-barrier structures, Phys. Rev. B **58**, 10619 (1998).

[44] A. Trita, I. Cristiani, V. Degiorgio, D. Chrastina, and H. von Känel, Measurement of carrier lifetime and interface recombination velocity in SiGe waveguides, Appl. Phys. Lett. **91**, 041112 (2007).

[45] M. Bonfanti, E. Grilli, M. Guzzi, M. Virgilio, G. Grosso, D. Chrastina, G. Isella, H. von Känel, and A. Neels, Optical transitions in Ge/SiGe multiple quantum wells with Ge-rich barriers, Phys. Rev. B **78**, 041407(R) (2008).

[46] S. A. Claussen, E. Tasyurek, J. E. Roth, and D. A. B. Miller, Measurement and modeling of ultrafast carrier dynamics and transport in germanium/silicon-germanium quantum wells, Opt. Express **18**, 25596 (2010).

[47] F. Pezzoli, F. Bottegoni, D. Trivedi, F. Ciccacci, A. Giorgioni, P. Li, S. Cecchi, E. Grilli, Y. Song, M. Guzzi, H. Dery, and G. Isella, Optical spin injection and spin lifetime in Ge heterostructures, Phys. Rev. Lett. **108**, 156603 (2012).

[48] A. Giorgioni, F. Pezzoli, E. Gatti, S. Cecchi, C. Kazuo Inoki, C. Deneke, E. Grilli, G. Isella, and M. Guzzi, Optical tailoring of carrier spin polarization in Ge/SiGe multiple quantum wells, Appl. Phys. Lett. **102**, 012408 (2013).

[49] C. Lange, G. Isella, D. Chrastina, F. Pezzoli, N. S. Köster, R. Woscholski, and S. Chatterjee, Spin band-gap renormalization and hole spin dynamics in Ge/SiGe quantum wells, Phys. Rev. B **85**, 241303(R) (2012).

[50] E. Gatti, E. Grilli, M. Guzzi, D. Chrastina, G. Isella, and H. von Känel, Room temperature photoluminescence of Ge multiple quantum wells with Ge-rich barriers, Appl. Phys. Lett. **98**, 031106 (2011).